Journal of Power Sources 222 (2013) 305–312

Contents lists available at SciVerse ScienceDirect

Journal of Power Sources

journal homepage: www.elsevier.com/locate/jpowsour

Carbon-supported nickel-doped manganese oxides as electrocatalysts for the oxygen reduction reaction in the presence of sodium borohydride

Amanda C. Garcia [a,b], Fabio H.B. Lima [a], Edson A. Ticianelli [a,*], Marian Chatenet [b]

[a] Instituto de Química de São Carlos, Universidade de São Paulo, Avenida Trabalhador Sãocarlense, 400 Parque Arnold Schmidt, CP 780, 13560-970 São Carlos, SP, Brazil
[b] Laboratoire d'Electrochimie et de Physico-chimie des Matériaux et des Interfaces LEPMI-Phelma, UMR 5279 CNRS/Grenoble, INP/U. de Savoie/U. Joseph Fourier BP 75, 38402 Saint Martin d'Hères Cedex, France

HIGHLIGHTS

- All (Ni)MnO_x catalysts are active for the oxygen reduction reaction.
- Ni segregate phases contribute to the BOR and the heterogeneous hydrolysis of BH_4^-.
- (Ni)MnO_x dispersed on E350G and MM225 carbons are not tolerant to BH_4^-.
- Low Ni-content (Ni)MnO_x dispersed on M1000 carbon is tolerant to BH_4^-.

ARTICLE INFO

Article history:
Received 26 June 2012
Received in revised form
16 August 2012
Accepted 17 August 2012
Available online 7 September 2012

Keywords:
Nickel-doped MnO_x electrocatalyst
Oxygen reduction reaction
Direct borohydride fuel cells
Differential electrochemical mass spectrometry

ABSTRACT

The electrocatalytic activity for the oxygen reduction reaction of nickel-doped MnO_x nanoparticles, dispersed onto different carbon powders (M1000, MM225 and E350) is studied in alkaline media in the presence of borohydride ions. Differential electrochemical mass spectrometry (DEMS) is used to quantify the H_2 yields coming from the borohydride hydrolysis as a function of the electrode potential. The polarization results show that materials containing Ni segregate phases present significant Faradaic currents for the borohydride oxidation, while the on-line DEMS results clearly evidence the production of H_2. For these electrocatalysts, the presence of BH_4^- induces a decrease of the overall ORR activity, and this is assigned, into a large extent, to a superposition of the ORR reduction currents with the currents related to the direct borohydride oxidation. This effect is far more pronounced for the electrocatalyst dispersed onto the E350 carbon. On the contrary, materials dispersed onto M1000 carbon and without Ni segregated phases seem tolerant to the presence of BH_4^- ions. Therefore, these materials may be an alternative to be used as cathode electrocatalysts of direct borohydride fuel cells.

1. Introduction

In the past few years, the increasing demand for portable electronic devices has stimulated the research for efficient, clean and high energy density electrical power sources such as fuel cells. In particular, alkaline fuel cells (AFC) present two major advantages over proton exchange membrane fuel cells [1,2]: (i) most reaction kinetics are faster in alkaline than in acid media; (ii) it is possible to use non-noble electrocatalysts without detrimental performance and stability losses. Normally, AFC are feed with hydrogen at the anode and oxygen at the cathode; the main problem with this is related to the hydrogen production and storage systems that complicate the fuel cell use in portable devices. It is considered that employing a liquid fuel to replace hydrogen for feeding the fuel cell anode would have many advantages in terms of the system simplicity, mass and volume, as well as for safety reasons [3], which is mandatory for nomad electronic devices. However, liquid fuels usually suffer major drawbacks: their electro-oxidation is generally slower than that of hydrogen and irreversible, as is the case of methanol [3,4] or ethylene glycol [5]. Moreover, these liquid fuels can diffuse through the electrolyte from the anode to the cathode and this process known as fuel crossover, greatly influences the oxygen reduction completion/kinetics [6].

Sodium borohydride ($NaBH_4$) may be an alternative fuel, thanks to its high capacity and energy density. Moreover, this fuel is non-toxic, easily stored as a powder and relatively stable in alkaline solution [7]. Amendola was the first that showed interest in the tetrahydroborate anion (BH_4^-) direct oxidation in a fuel cell anode

* Corresponding author. Tel.: +55 16 3373 9945; fax: +55 16 3373 9952.
E-mail address: edsont@iqsc.usp.br (E.A. Ticianelli).

0378-7753/$ – see front matter © 2012 Elsevier B.V. All rights reserved.
http://dx.doi.org/10.1016/j.jpowsour.2012.08.049

instead of hydrogen [8]. The anode compartment of the so-called direct borohydride fuel cell (DBFC) is then fed with an alkaline solution of sodium borohydride, which may suffer spontaneous reaction with water for pH < 12, but is rather stable regarding such homogeneous hydrolysis above pH 12 [9,10]. However, the borohydride oxidation reaction (BOR) is a complex eight-electron process [7,11] (Eq. (1)) and its kinetics and mechanistic pathways depend on several variables such as the composition of the solution (pH, $[BH_4^-]$, etc.), the catalyst material and the temperature [12].

$$BH_4^- + 8OH^- \rightarrow BO_2^- + 6H_2O + 8e^- \quad E_0 = -1.24\ V_{NHE} \qquad (1)$$

Nevertheless, depending on the electrode material (example Au and Pt), the eight-electron BOR may compete with the quasi-spontaneous heterogeneous hydrolysis of Eq. (2) at the electrode [12].

$$BH_4^- + 2H_2O \rightarrow BO_2^- + 4H_2 \qquad (2)$$

The occurrence of this latter reaction actually lowers the practical number of electrons exchanged per BH_4^- anion because it generates H_2 at a rather uncontrolled rate, some of which being prone to evolve away from the electrode without being oxidized. As a result, the overall Faradaic efficiency of the electrocatalyst decreases [13]. On the contrary, if the residence time of the hydrogen gas generated by the heterogeneous hydrolysis increase in the electrocatalytic site, and if the electrocatalyst is capable of oxidizing H_2 (Eq. (3)), higher Faradaic efficiency can be obtained, as demonstrated by Chatenet et al. for Pt/C active layers of various thicknesses [14,16].

$$H_2 + 2OH^- \rightarrow 2H_2O + 2e^-, E_0 = -0.83\ V_{NHE} \qquad (3)$$

Another issue related to the DBFC is linked to the BH_4^- crossover to the cathode compartment, as mentioned above for other direct liquid fuel cells. This issue was already studied in a previous paper, where nanometric MnO_x/C, either undoped or doped by magnesium cations included in the MnO_x lattice was investigated as electrocatalyst for the oxygen reduction reaction (ORR) in the presence of BH_4^-. It was found that these materials could consist of relevant ORR electrocatalysts in BH_4^- containing alkaline solution, since they seemed rather tolerant to borohydride species [16,17]. The present contribution reports the use of nickel-doped MnO_2-catalysts supported on different types of high-surface area carbon substrates as electrocatalysts for the ORR in the presence of sodium borohydride. These electrocatalysts have shown very high electrocatalytic activity for ORR [19] and it would be of interest to check the influences of (i) doping the MnO_x phase with nickel cations and (ii) using different types of carbon supports, on the electro-oxidation and/or the catalytic decomposition of BH_4^- anions [17,18], as well as on tolerance of the ORR to the presence of BH_4^-. Ni has been chosen as dopant for MnO_x/C, because it stabilizes the Mn^{IV}/Mn^{III} transition, which is an active center for the ORR [19,20]. In addition, the 4-electron ORR pathway is favored in such materials [19,21].

The present paper, therefore, investigates the ORR on such $NiMnO_x$/C electrocatalysts in the presence or absence of BH_4^- in the alkaline solution. Their activity toward the borohydride oxidation reaction (BOR) was studied by comparing the ORR polarization plots with/without $NaBH_4$ in solution. Also, it was investigated their role in the heterogeneous hydrolysis of BH_4^- using a technique enabling the direct quantification of H_2 resulting from that catalytic reaction, namely, on-line *differential electrochemical mass spectrometry* (DEMS). The so-obtained sets of data enabled the study of the BH_4^- tolerance of this family of $NiMnO_x$/C materials when used for the ORR in alkaline solutions containing $NaBH_4$.

Table 1
Composition (obtained by ICP-AES analyses), and presence/absence of Ni segregated phase (as detected from XRD) for the various $NiMnO_x$-based materials [21]. The wt.% MnO_2 values were calculated assuming that each Mn atom is combined with 2 O atoms to form a MnO_2 moiety.

Catalyst/ Carbons	Composition				Presence of Ni segregated phase (XRD)
	wt.% Ni	wt.% Mn	wt.% MnO_2	wt.% MnO_2 + Ni	
M1000 – 2.0 g Ni	2.2	8.6	13.6	16.0	Yes
M1000 – 0.2 g Ni	0.5	11.6	18.4	19.0	No
MM225 – 0.2 g Ni	0.7	18.0	28.3	29.0	Yes
E350 – 0.2 g Ni	0.3	12.8	20.2	20.5	Yes

2. Experimental procedures

2.1. Synthesis and physicochemical characterizations of MnO_x/C-based catalysts

The carbon-supported nickel-doped nanometric manganese oxides ($NiMnO_x$/C, C = M1000 (Monarch 1000 – Cabot), MM225 and E350 (both from Timcal)) were prepared by a mild hydrothermal treatment first described by Bezdicka et al. [15]. The as-obtained electrocatalysts were thoroughly characterized in a previous paper [21]. For clarity, their physicochemical properties are summarized in Table 1.

2.2. Electrocatalytic activity of the carbon-supported Ni-doped MnO_x/C-based for the ORR

The working electrodes for the electrocatalytic tests of the ORR were formed by ultra thin-layer deposits of the catalysts onto a glassy carbon disk ($\phi = 5$ mm, $A = 0.196\ cm^2$) inserted in a Teflon cylinder cup of a rotating disk electrode (RDE) (Pine Instruments) [22]. For the preparation of these catalytic layers, a suspension composed of 2.0 mg of the MnO_x/C or $NiMnO_x$/C powders, 1.0 mL isopropyl alcohol, and 20 μL of Nafion 5.0 wt.% was used. After ultrasonic homogenization, 20 μL drop of the ink was deposited on the glassy carbon electrode, and the solvent was evaporated at room temperature. All solutions were prepared with (18.2 MΩ cm, <5 ppb Total Organic Carbon) ultra-pure water (Millipore, Elix + Milli-Q gradient) and 1.0 mol L^{-1} sodium hydroxide (99.99%, Aldrich) containing or not 10^{-3} mol L^{-1} sodium borohydride (Merck, Suprapur).

The electrochemical experiments were conducted using a PGSTAT 20 potentiostat (Autolab) in a conventional three-electrode cell, and in 1.0 mol L^{-1} NaOH electrolyte. A gold foil was used as the counter electrode. The use of gold electrode prevents the strong borohydride hydrolysis that would result from the use of platinum electrodes in the open circuit potential [7,9,23]. The reference was $Hg/HgO/OH^-$ in 1.0 mol L^{-1} NaOH.

Blank currents of the $NiMnO_x$/C materials were obtained by cyclic voltammetry (CV) in the range −0.88 to 0.5 V *vs.* $Hg/HgO/OH^-$ (5.0 mV s^{-1}, in the presence and absence of 10^{-3} mol L^{-1} $NaBH_4$), carried out after degassing the solution with argon. Oxygen reduction voltammetry experiments were performed after oxygen saturation of the electrolyte (containing or not 10^{-3} mol L^{-1} sodium borohydride) during 40 min. The oxygen concentration was kept constant at its saturation value by gentle but permanent O_2-bubbling in solution during the measurements. Quasi-steady-state ORR voltammograms were recorded at 5.0 mV s^{-1} from 0.5 to −0.88 V *vs.* $Hg/HgO/OH^-$ for RDE rotation speeds in the range of

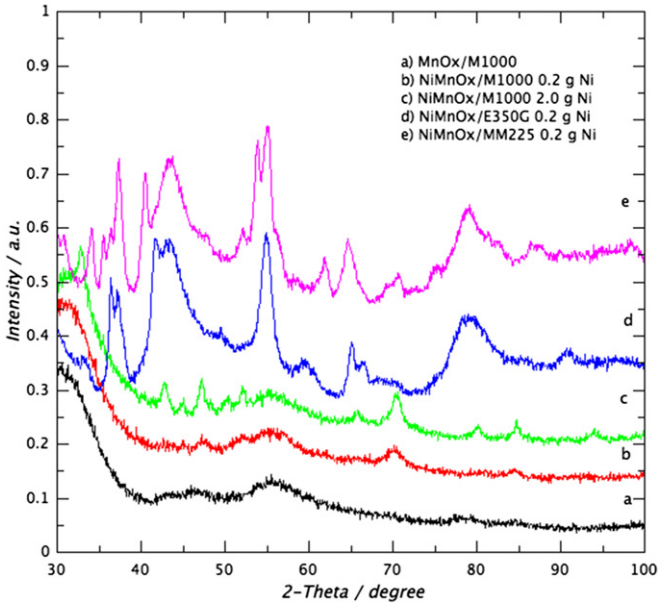

Fig. 1. Examples of X-ray diffraction (Fe Kα radiation) patterns for representative materials: MnO_x supported on M1000, E350, and MM225 carbons with different Ni loads.

100–2500 rpm. Prior to each experiment, the potential was kept for 2 min at the starting potential of 0.5 V *vs.* Hg/HgO/OH^-, to ensure an identical initial state of surface for the $NiMnO_x$/C materials in all experiments.

2.3. Differential electrochemical mass spectrometry (DEMS)

DEMS measurements were performed with a Pfeiffer-Vacuum QMA 200 quadrupole mass spectrometer using a setup consisting of two differentially pumping chambers. Details of this method are given elsewhere [24,25]. The method allows the on-line detection of volatile and gaseous products of electrochemical reactions during the application of a potential scan. In a typical DEMS experiment, the current *vs.* potential curves are recorded simultaneously with the mass intensity *vs.* potential curves, for selected values of m/z (mass/charge) ionic signals.

The working electrodes (WE) for the DEMS measurements were prepared by pipetting and drying 60 μL of the different Ni-doped MnO_x-based catalyst aqueous suspension of 2 mg mL^{-1}, and then, 20 μL aqueous Nafion solution in the center of a glassy carbon disk (9 mm in diameter).

The glassy carbon electrode was mounted into a dual thin-layer flow cell ("wall-jet" geometry) [22,26] and pressed against a *ca.* 50 μm thick Teflon spacer, resulting in an exposed area of 0.28 cm^2 and an electrolyte volume of *ca.* 5 μL. In present configuration, the electrolyte flow was driven by the hydrostatic pressure in the supply bottle (flow rate of *ca.* 10–15 μL s^{-1}) first entering in the thin-layer compartment in front of the electrode ("wall-jet" geometry) and then flowing through one of four capillaries into the lower compartment ("detection cell"), where volatile products can reach the porous Teflon membrane (Gore-Tex® PTFE – thickness of 50 μm and pore size of 0.02 μm). The DEMS measurements were performed for $m/z = 2$ (the H_2 signature) and piloted by the Quadstar software (Pfeiffer-Vacuum).

The WE was connected to the potentiostat *via* a gold current collector. It is wise to point here that there was no contact between the gold wire and the solution, so the gold wire did not promote any heterogeneous hydrolysis of $NaBH_4$ [8]. The counter electrode was formed by two Au wires at the inlet and outlet of the thin-layer cell, connected through a controllable external resistance (500 k ohm), and a Hg/HgO/OH^- in the same electrolyte served as the reference electrode. All DEMS measurements were performed at room temperature (25 ± 2 °C) after degassing the solution with argon, using a PGSTAT 20 potentiostat (Autolab) connected to the four-electrodes spectroelectrochemical cell. Benchmark cyclic voltammograms were also plotted in the 1.0 mol L^{-1} NaOH bare electrolyte in the range from −0.88 to 0.5 V *vs.* Hg/HgO/OH^- at 10 mV s^{-1}. Prior to each voltammetric cycle, the potential was kept for 2 min at the starting potential, −0.88 V *vs.* Hg/HgO/OH^-, to ensure an identical initial state of surface for the $NiMnO_x$/C materials, and to stabilize the baseline in the MS measurements.

3. Results and discussion

3.1. Physicochemical characterizations of the MnO_x/C-based catalysts

Table 1 shows a summary of the chemical/physicochemical properties of the catalysts obtained previously by several techniques [19]. Firstly, HRTEM images [19] showed that the materials dispersed onto M1000 carbon with a 2.0 g Ni load (20 wt.%), MM225 and E350 (both with 0.2 g Ni) are in the form of nanocrystalline agglomerates, while catalysts dispersed onto M1000 (0.2 g Ni) are in the form of highly oriented nanocrystalline needles. Fig. 1 shows the XRD profiles for all materials. For $NiMnO_x$/M1000 (2.0 g Ni) and $NiMnO_x$/C (C = MM225 and E350) 0.2 g Ni, the profiles exhibit small but consistent reflections associated to Ni and NiO segregated phases at 2θ = 48, 55, 56, 66, 82 degree (Fe Kα radiation), while for the $NiMnO_x$/M1000 0.2 g Ni material the XRD spectrum evidences that the nickel divalent cations were nearly completely inserted into the MnO_x phase, leaving no apparent Ni or NiO segregated phases. These observations are summarized in Table 1.

3.2. Electrocatalytic activity for the oxygen reduction reaction

Fig. 2 compares the polarization behavior of the MnO_x/C-based electrocatalysts for the ORR in the absence and in the presence of sodium borohydride. In absence of BH_4^-, for all MnO_x-based electrocatalysts, the quasi-stationary ORR voltammograms show the classical diffusion–convection plateaus observed in RDE experiments. In the present experimental conditions, the onset of the oxygen reduction wave is similar for all materials, independent of the Ni load and of the carbon substrate.

As discussed in previous published papers [27–30], manganese oxide-containing materials would reduce oxygen to peroxide species at high potential (low ORR overpotential), and this is followed by heterogeneous catalytic chemical disproportionation reaction of HO_2^-. The extent of such heterogeneous reaction depends on the catalyst composition and morphology [31] and also on the catalyst load in the thin porous coating (tpc) layer. In this work the different limiting current densities observed in Fig. 2 for the different catalysts can be primarily inferred to the different loads of the catalyst powders into the tpc layers, which result in different residence times of the HO_2^- species inside this layer thus resulting on different extension of the disproportionation reaction.

Fig. 2 also displays the influence of the nature of the $NiMnO_x$/C materials (*i.e.* of their morphology/composition that may depend on the carbon substrate and Ni and Mn loadings) on the behavior toward the ORR in the presence of BH_4^-. In all cases, the limiting current plateaus are well defined, except for materials dispersed onto E350 carbon (Fig. 2a). The results indirectly show that the

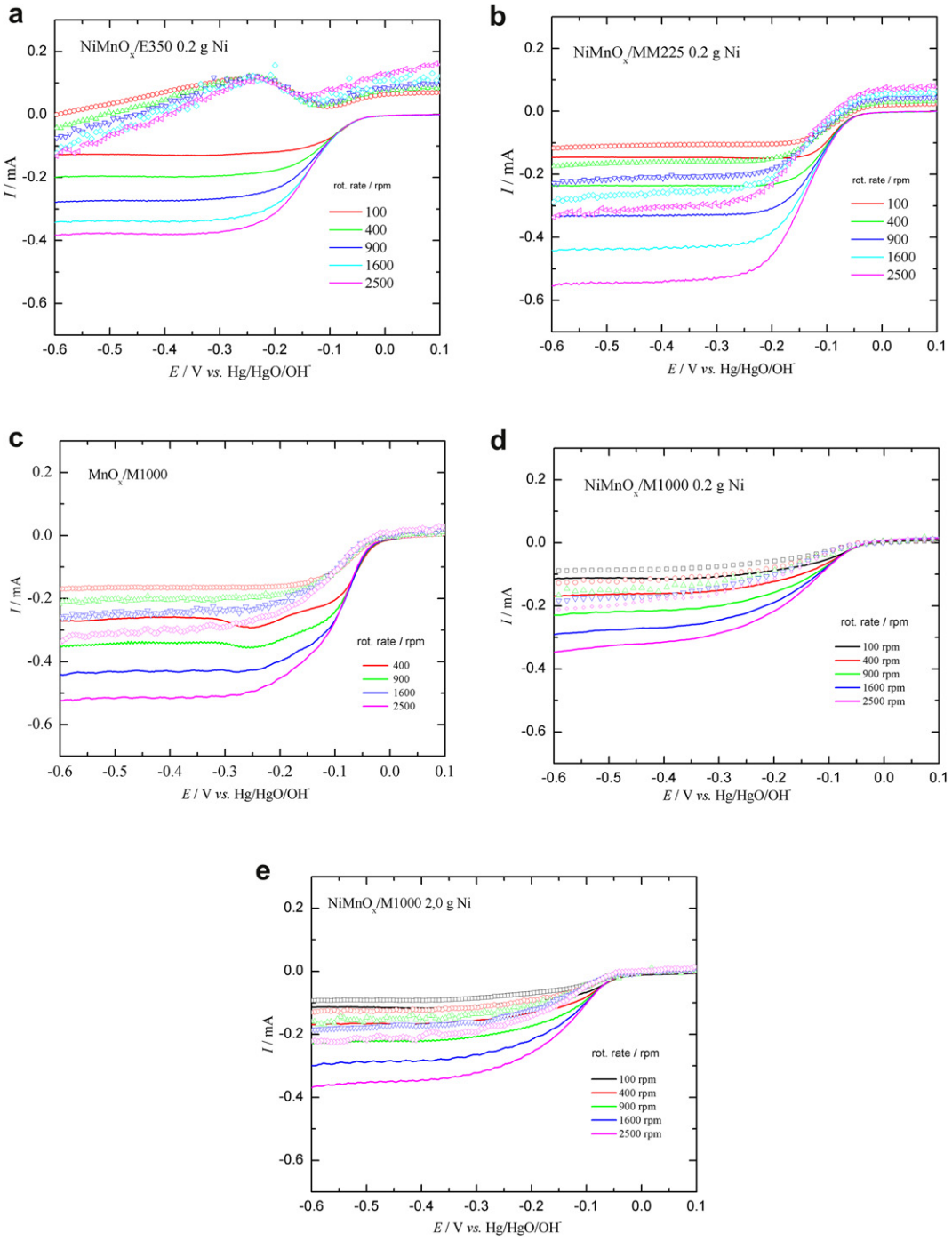

Fig. 2. Oxygen reduction reaction (ORR) voltammograms (5.0 mV s^{-1}) obtained on MnO_x-based electrocatalysts in the RDE setup. (symbol) in 1.0 mol L^{-1} NaOH + 10^{-3} mol L^{-1} $NaBH_4$ and (lines) in 1.0 mol L^{-1} NaOH. Electrode geometric area: 0.196 cm^2.

number of electrons involved in the ORR decreases in all cases when BH_4^- anions are present in the solution. This means that the presence of BH_4^- ion modifies the current produced in the cathode for all electrocatalysts, and this effect is more pronounced for the electrocatalyst dispersed onto E350 carbon.

Aiming at understanding these results, the BOR was investigated in the absence of oxygen, either for the bare carbon substrates (MnO_x-free) and for the MnO_x-based catalysts, and obtained curves are shown in Figs. 3 and 4, respectively. In particular for NiMnO$_x$/E350 0.2 g Ni, comparing the results of Figs. 2–4, it can be clearly noted that this material is active for both the ORR and the BOR. Therefore, it can be proposed that the above-mentioned decrease of the number of electrons during the ORR results, into a large extent, from the superposition of the (negative) ORR reduction currents with the (positive) currents related to the borohydride oxidation. Knowing that the BH_4^- crossover would be nearly unavoidable in an operating DBFC, it must be concluded that this electrocatalyst, although very relevant from its intrinsic ORR performances [18], is unusable for the cathode of a DBFC. Firstly, its ORR activity is immensely perturbed by BH_4^- and, secondly, BH_4^-

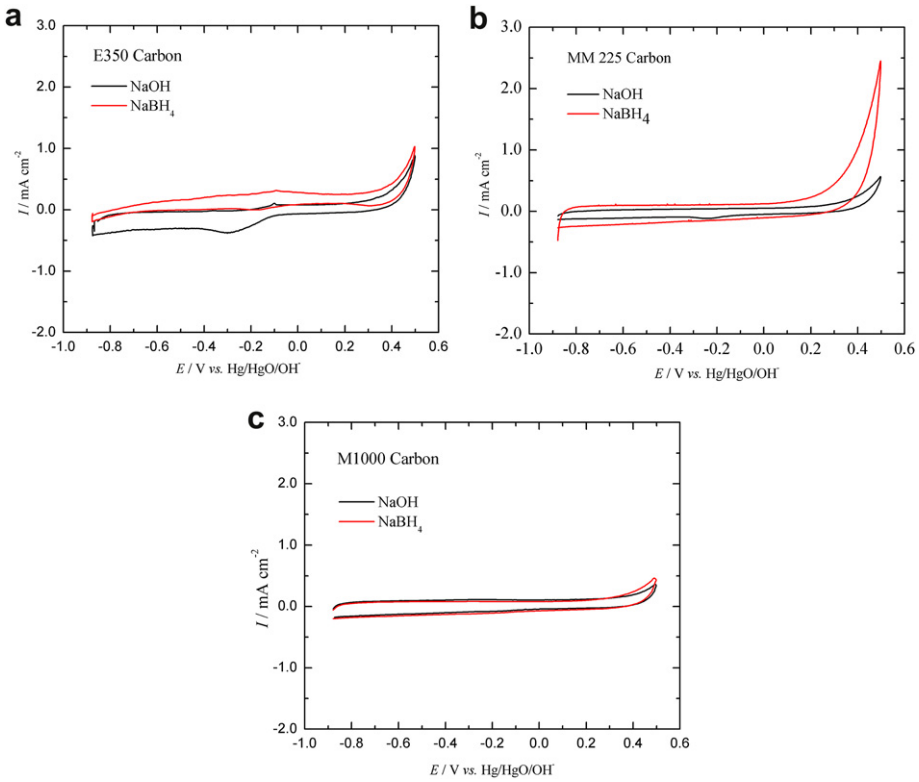

Fig. 3. Cyclic voltammograms plotted at 5.0 mV s^{-1} in the absence of any O_2 in solution for the three bare carbon substrates in the presence and absence of 10^{-3} mol L^{-1} $NaBH_4$ in the 1.0 mol L^{-1} NaOH supporting electrolyte. Electrode geometric area: 0.196 cm^2.

species would be inevitably consumed in the cathode, thereby affecting the Faradaic efficiency of the system. This special behavior for this electrocatalyst is surely related to its composition and morphology. The XRD spectra (Fig. 1) showed isolated Ni and NiO phases, and Ni is active for the borohydride oxidation reaction and hydrolysis [17–19], as will be explained later. Additionally, the results obtained using pure E350 carbon electrodes (Fig. 3a) also showed non-negligible activity toward the BOR. So, it is likely that the increase in the Faradaic current reported in Fig. 4a also contains some contribution of the E350 carbon itself, but this is not very large. In summary, the presence of the Ni-containing phases primarily explains the inadequate behavior of the $NiMnO_x$/E350 0.2 g Ni electrocatalyst toward the ORR in the presence of BH_4^-.

For the $NiMnO_x$/MM225 0.2 g Ni electrocatalyst, the polarization results showed some decrease in the values of the ORR limiting current in the presence of BH_4^-, evidencing a decrease in the number of electrons exchanged during the oxygen reduction. Figs. 3b and 4b clearly indicate the appearance of anodic currents related to borohydride electro-oxidation. Therefore, the decrease of the value of ORR limiting current due to the presence of BH_4^- can be associated to the non-negligible activity of $NiMnO_x$/MM225 0.2 g Ni for the BOR, although the possibility of a change of ORR mechanism cannot be excluded (see below). Here again, the catalyst behavior with respect to the BOR can be associated to the morphology and composition of the material, particularly to the presence of Ni segregated phases, as evidenced by XRD [19]. Also, as in the case of E350, the pure MM225 carbon support displays very little activity toward the BOR (Fig. 3b), showing that also in this case the activity toward the BOR of the $NiMnO_x$/MM225 material may only be ascribed to the presence of the Ni segregated phases.

The catalysts dispersed onto M1000 carbon supports show different behaviors regarding the BOR, depending on the presence of Ni in the MnO_x/C phase. In absence of Ni (MnO_x/M1000, Fig. 4c), the presence of BH_4^- anions in solution seems to reduce part of the MnO_2 phase to MnOOH and, then, to Mn_3O_4 which is electrochemically inactive [32], causing a reduction of the CV current, but no BH_4^- oxidation currents were observed. For the M1000 material containing 0.2 g Ni (Fig. 4d), the results also evidence no oxidation currents for the BOR, and the reason for this may be related to the fact that the divalent Ni cation is completely inserted into the MnO_x crystal structure, as shown by XRD (Fig. 1), not being available for the borohydride adsorption. On the contrary, in the case of $NiMnO_x$/M1000 2.0 g Ni (Fig. 4e) the material promotes the BH_4^- oxidation, as for the other materials, and this seems to be due to the presence of Ni segregated phases, as also evidenced by the XRD spectrum.

Surprisingly, these very different behaviors in the absence of oxygen in solution (Fig. 4c–e) are not yielding dramatic differences in the ORR voltammograms (Fig. 2c–e). In the cases of the electrocatalysts dispersed onto M1000 carbons, the presence of BH_4^- causes a decrease of the values of the limiting currents for the ORR and just a small shift of the reaction onset potential to more negative values. Overall, these changes seem rather mild compared to those observed when E350 carbon substrate is used, and express a partial tolerance of these (Ni)MnO_x/M1000 electrocatalysts to BH_4^-, as was previously noted for similar nanostructured (Mg) MnO_x/C materials supported on another type of carbon black (Chezacarb) [33]. Nevertheless all materials that promote the BH_4^- oxidation, like $NiMnO_x$/M1000 2.0 g Ni and $NiMnO_x$/E350 and MM225 0.2 g Ni, have a common feature, that is, the BOR onset potential locates at *ca.* −0.4 V *vs.* Hg/HgO/OH^-, expressing a reasonably large activity for the BOR.

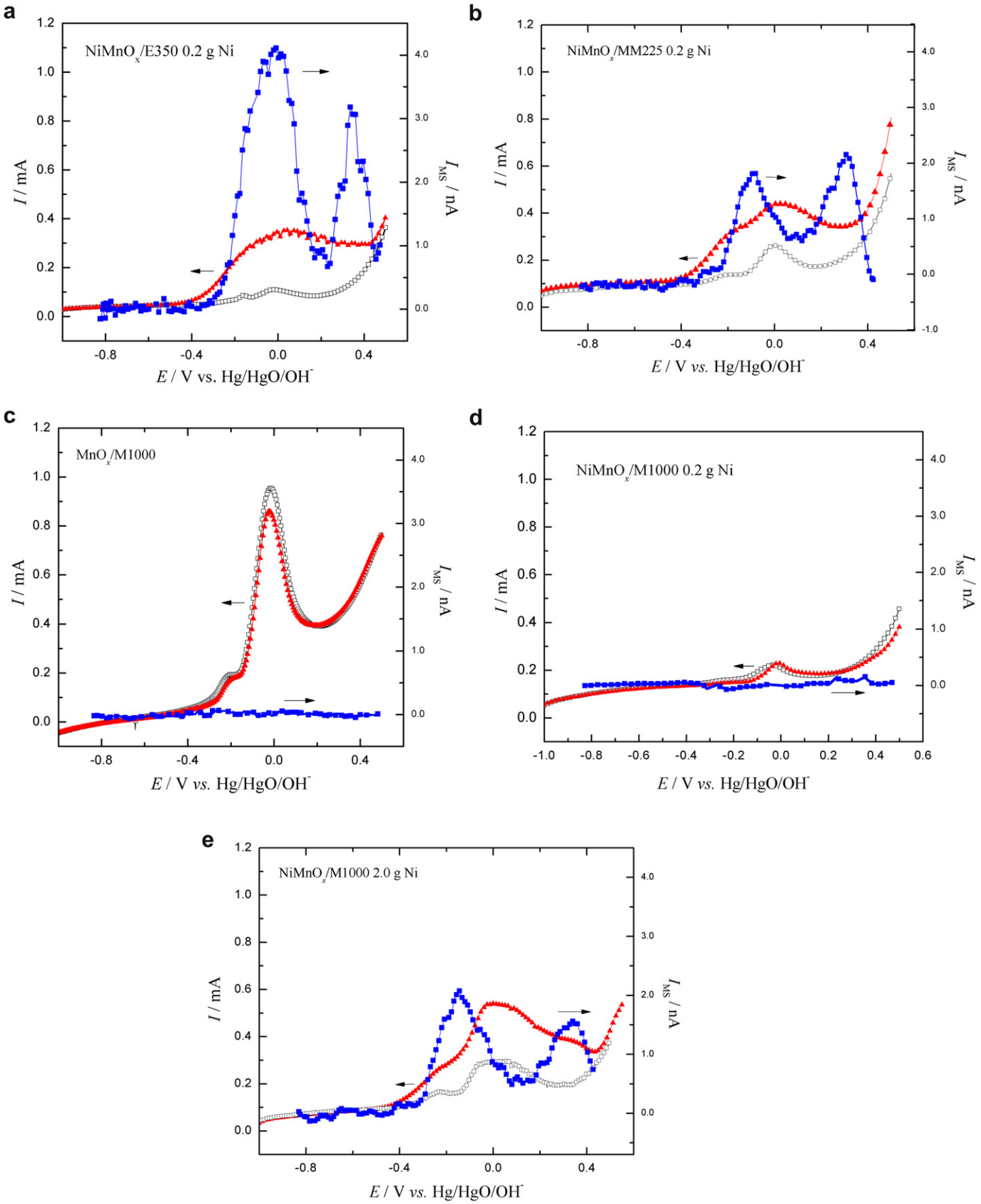

Fig. 4. Faradaic and ionic currents for H_2 formation ($m/z = 2$) obtained in DEMS experiments during CV (positive-going scan) of borohydride electro-oxidation reaction catalyzed by the different investigated MnO_x-based electrocatalysts, in the presence (triangles) and absence (squares) of 10^{-3} mol L^{-1} $NaBH_4$ in the 1.0 mol L^{-1} NaOH supporting electrolyte. Scan rate of 5.0 mV s^{-1}.

3.3. Reactions and mechanisms

A mechanistic analysis of the ORR in the different investigated catalysts was made previously in terms of mass-transport-corrected Tafel plots (E *vs.* $\log[i_k = (i \times i_d)/(i_d - i)]$, where i_d is the diffusion limiting current) [34]. The Tafel coefficients for the ORR confirmed the rather identical bulk kinetic activity of the various manganese oxide-based materials in absence of BH_4^- ion. However, there are important differences in the values of the Tafel slopes, which were found around 90 mV dec^{-1} for the M1000-based materials and around 50–55 mV dec^{-1} for the MM225 and E350 electrocatalysts. These results would evidence a very little participation of the carbon particles in the oxygen reduction electrocatalysis for the M1000 carbon, while in the other two cases, the participation may be more significant and, thus, the Tafel slopes resulted closer to that of pure carbon in the same electrolyte (30 mV dec^{-1}) [35]. This observation is consistent with the large surface area of these carbons [19]. It has to be also noted that the presence of different phases of Mn oxides in the $NiMnO_x$/MM225 and $NiMnO_x$/E350 materials compared to that on M1000 may also be responsible for the differences in the Tafel slopes.

As mentioned before, it is commonly accepted that all MnO_x/C-based materials, in absence of BH_4^-, would reduce oxygen with peroxide formation [19–21]

$$O_2 + H_2O + 2e^- \rightarrow HO_2^- + OH^- \quad (5)$$

followed by heterogeneous catalytic chemical disproportionation reaction of HO_2^-:

$$2HO_2^- \rightarrow O_2 + 2OH^- \quad (6)$$

However, in the presence of the borohydride ions, the characterization of the oxygen reduction reaction mechanism on these materials becomes difficult. In order to better understand the role of the BH_4^- on the electrocatalysis of this reaction, the DEMS technique was used to quantify the H_2 ($m/z = 2$) yields coming from the borohydride hydrolysis (Eq. (2)) as a function of the electrode potential. These results are also displayed in Fig. 4 for all catalysts, together with the corresponding anodic CV responses (positive-going scan) in the absence and in the presence of borohydride ions.

The on-line DEMS results confirm the great impact of the composition/morphology of the various (Ni)MnO_x/C electrocatalysts also on the hydrogen production. For materials containing the Ni segregate phases, which presents Faradaic current for the BOR, the on-line DEMS results clearly evidence the production of H_2, as are the cases of $NiMnO_x$/C (C = E350 and MM225) 0.2 g Ni and $NiMnO_x$/M1000 2.0 g Ni catalysts (Fig. 4a, b and e). In these cases, the DEMS results exhibited an ion current signal referred to the molecular hydrogen ($m/z = 2$) for potentials higher than *ca.* −0.4 V *vs.* Hg/HgO/OH^-, presenting a maximum at *ca.* −0.1 V; after that, the current decreases but around 0.2 V it increases again showing another peak at *ca.* 0.3–0.4 V.

It is wise to point out that the first peak of the $m/z = 2$ signal coincides with the onset of the Faradaic current of borohydride oxidation (Fig. 4). Similar result for the H_2 production during the BOR was obtained on Au [36]. So, it can be stated that the H_2 formation takes place according to the following steps:

$$BH_4^- + H_2O \rightarrow BH_3OH_{ad}^- + H_2 \quad (7)$$

Followed by:

$$BH_3OH_{ad}^- \rightarrow BH_2OH_{ad} + (1/2)H_2 + e^- \quad (8)$$

The first hydrolysis step may occur due to the chemical reduction of the Ni-oxide species back to metallic Ni, by BH_4^-, producing BH_3OH^- and H_2. This is accompanied by the electrochemical oxidation of the BH_3OH^- species on the surface of metallic Ni atoms, producing additional H_2 molecules (Eq. (8)), which is responsible for the massive H_2 detection during the DEMS measurements. After the anodic peak of the Faradaic oxidation of borohydride on the Ni-containing active materials, the Ni atoms may suffer electro-oxidation due to the high electrode potential values. This is followed by chemical reduction of the just formed Ni-oxides by the incoming borohydride ions from the electrolyte, producing H_2 molecules, following a reaction similar to that presented in Eq. (7). This last step may be responsible for the second ionic current peak of the $m/z = 2$ signal, observed in Fig. 4a, b and e. Therefore, the on-line DEMS results confirmed that the presence of Ni segregated phase is crucial for the electrocatalyst activity for the BOR.

In summary, the present results indicate that, for most MnO_x-based electrocatalysts, the decrease of the overall ORR activity arises into a large extent, from a superposition of the (negative) ORR reduction currents with the (positive) currents related to the directly borohydride oxidation. In Fig. 2, it is seen that, except for $NiMnO_x$/E350 0.2 g Ni, the main effect of BH_4^- in the ORR polarization curves is a lowering of the limiting currents. So, in these cases, one can argue that the actual O_2 concentration in the thin porous coating layer may be lowered because of its chemical catalytic reduction by the borohydride and/or hydrogen species generated by the hydrolysis, promoted at the catalyst surface. Another possibility is that the HO_2^- disproportionation reaction (Eq. (6)) may be disturbed because of a possible reaction of HO_2^- with BH_4^- or H_2.

4. Conclusions

It was studied the selectivity for oxygen reduction reaction in the presence of sodium borohydride in alkaline medium for various electrocatalysts materials. Overall, the present results demonstrate the great impact of the morphology/composition of the $NiMnO_x$/C materials on the ORR in the presence of BH_4^- ion. The results seem to show that the presence of Ni segregate phase contributes to the BOR and the heterogeneous hydrolysis of BH_4^-, because nickel intrinsically possesses non-negligible activity toward these reactions. In addition, (Ni)MnO_x electrocatalysts dispersed onto E350 and MM225 carbons are not tolerant to the presence of BH_4^-, but this is much less important for the MM225 than for the E350 substrate; therefore, none of these materials are good catalysts for the DBFC cathode. On the contrary, materials dispersed onto M1000 carbon seem tolerant to the presence of $NaBH_4$ when the "composition" of the $NiMnO_x$ particles is relevantly chosen (*i.e.* without Ni segregated phase – (Ni)MnO_x 0.2 g Ni); then, this catalysts may be an alternative to be used at the cathode of a direct borohydride fuel cell.

Acknowledgments

The authors thank CNPq, Capes/Cofecub (project Ph 598/08) and FAPESP for financial supports.

References

[1] D.B. Meadowcroft, Nature 226 (1970) 847.
[2] M. Maja, C. Orechia, M. Strano, P. Tosco, M. Vanni, Electrochim. Acta 46 (2000) 423.
[3] W. Vielstich, A. Lamm, H.A. Gasteiger, Handbook of Fuel Cells, vol. 5, Wiley-UK, Chichester, 2003.
[4] R.X. Feng, H. Dong, Y.D. Wang, Electrochem. Commun. 7 (2005) 449.
[5] K. Matsuoka, Y. Iriyama, T. Abe, M. Matsuoka, Z.J. Oguma, J. Power Sourc. 150 (2005) 27.

[6] F. Maillard, M. Martin, F. Gloaguen, J.M. Léger, Electrochim. Acta 47 (2002) 3431–3440.
[7] J.H. Morris, H.J. Gysling, D. Reed, Chem. Rev. 85 (1985) 51–76.
[8] S.C. Amendola, S. C, US Patent 5, 804, 329, 1998.
[9] S. Ozkar, M.J. Zahmakiran, J. Alloys Compd. 728 (2005) 404–406.
[10] J.A. Gardiner, J.W. Collat, J. Am. Chem. Soc. 87 (1965) 1692.
[11] S.C. Amendola, P. Onnerud, M.T. Kelly, P.J. Petillo, S.L. Sharp-Goldman, M. Binder, J. Power Sourc. 84 (1999) 130–133.
[12] B. Molina Concha, M. Chatenet, F. Maillard, E.A. Ticianelli, F.H.B. Lima, R.B. de Lima, Phys. Chem. Chem. Phys. 12 (2010) 11507.
[13] M. Chatenet, F.H.B. Lima, E.A. Ticianelli, J. Electrochem. Soc. 157 (2010) B697–B704.
[14] B. Molina Concha, M. Chatenet, Electrochim. Acta 54 (2009) 6130.
[15] P. Bezdicka, T. Grygar, B. Klápště, J. Vondrák, Electrochim. Acta 45 (1999) 913.
[16] K.S. Freitas, B.M. Concha, E.A. Ticianelli, M. Chatenet, Catal. Today 170 (2011) 110–119.
[17] B.H. Liu, Z.P. Li, S. Suda, J. Electrochem. Soc. 150 (2003) A398–A402.
[18] B.H. Liu, Z.P. Li, S. Suda, J. Alloys Compd. 415 (2006) 288–293.
[19] J. Vondràk, B. Klápště, J. Velická, M. Sedlaříková, V. Novàk, J. Reiter, J. New Mater. Electrochem. Syst. 8 (2005) 1.
[20] I. Roche, E. Chainet, M. Chatenet, J. Vondrák, J. Phys. Chem. C 111 (2007) 1434–1443.
[21] A.C. Garcia, A.D. Herrera, E.A. Ticianelli, M. Chatenet, C. Poinsignon, J. Electrochem. Soc. 158 (3) (2011) B290–B296.
[22] J.P. Hoare, The Electrochemistry of Oxygen, John Wiley & Sons, New York, 1968, p. 18.
[23] M.V. Mirkin, H. Yang, A.J. Bard, J. Electrochem. Soc. 139 (1992) 2212.
[24] H. Baltruschat, J. Am. Soc. Mass. Spectrom. 15 (2004) 1693.
[25] J.P.I. de Souza, S.L. Queiroz, F.C. Nart, Quimica Nova 23 (2000) 384.
[26] H. Wang, Z. Jusys, R.J. Behm, J. Power Sourc. 154 (2006) 351.
[27] F.H.B. Lima, M.L. Calegaro, E.A. Ticianelli, J. Electroanal. Chem. 590 (2006) 152.
[28] M.L. Calegaro, F.H.B. Lima, E.A. Ticianelli, J. Power Sourc. 158 (2006) 735.
[29] F.H.B. Lima, M.L. Calegaro, E.A. Ticianelli, Electrochim. Acta 52 (2007) 3732.
[30] F.H.B. Lima, M.L. Calegaro, E.A. Ticianelli, Russ. J. Electrochem. 42 (12) (2006) 1417.
[31] L. Mao, D. Zhang, T. Sotomura, K. Nakatsu, N. Koshiba, T. Ohaka, Electrochim. Acta 48 (2003) 1015.
[32] J. McBreen, Electrochim. Acta 20 (1975) 221.
[33] M. Chatenet, F. Micoud, I. Roche, E. Chainet, J. Vondrak, Electrochim. Acta 51 (2006) 5452–5458.
[34] J.-P. Diard, B. Le Gorrec, C. Montella, Cinétique Electrochimique, Herman, Paris, 1996.
[35] J. Perez, E.R. Gonzalez, E.A. Ticianelli, Electrochim. Acta 44 (1998) 1329.
[36] F.H.B. Lima, A.M. Pasqualeti, M.B. Molina Concha, M. Chatenet, E.A. Ticianelli, Electrochim. Acta, in press.